



## Paclitaxel loaded liposomes decorated with a multifunctional tandem peptide for glioma targeting



Yayuan Liu, Rui Ran, Jiantao Chen, Qifang Kuang, Jie Tang, Ling Mei, Qianyu Zhang, Huile Gao, Zhirong Zhang, Qin He\*

Key Laboratory of Drug Targeting and Drug Delivery Systems, West China School of Pharmacy, Sichuan University, No. 17, Block 3, Southern Renmin Road, Chengdu 610041, PR China

### ARTICLE INFO

#### Article history:

Received 23 December 2013

Accepted 20 February 2014

Available online 17 March 2014

#### Keywords:

Tandem peptide  
Cell penetrating peptide  
BBB penetrating  
Glioma targeting

### ABSTRACT

The treatment of glioma is a great challenge because of the existence of the blood-brain barrier (BBB). In order to reduce toxicity to the normal brain tissue and achieve efficient treatment, it is also important for drugs to specifically accumulate in the glioma foci and penetrate into the tumor core after entering into the brain. In this study, a specific ligand cyclic RGD peptide was conjugated to a cell penetrating peptide R8 to develop a multifunctional peptide R8-RGD. R8-RGD increased the cellular uptake of liposomes by 2-fold and nearly 30-fold compared to separate R8 and RGD respectively, and displayed effective penetration of three-dimensional glioma spheroids and BBB model *in vitro*. *In vivo* studies showed that R8-RGD-lipo could be efficiently delivered into the brain and selectively accumulated in the glioma foci after systemic administration in C6 glioma bearing mice. When paclitaxel (PTX) was loaded in liposomes, R8-RGD-lipo could induce the strongest inhibition and apoptosis against C6 cells and finally achieved the longest survival in intracranial C6 glioma bearing mice. In conclusion, all the results indicated that the tandem peptide R8-RGD was a promising ligand possessing multi functions including BBB transporting, glioma targeting and tumor penetrating. And R8-RGD-lipo was proved to be a potential anti-glioma drug delivery system.

© 2014 Elsevier Ltd. All rights reserved.

### 1. Introduction

Glioma is considered as the most aggressive primary malignant tumor of the brain. The treatment of glioma with lower side effects remains a great challenge because of the existence of several barriers. The first obstacle for a brain drug delivery system to conquer is the blood–brain barrier (BBB), which prevents nearly all large-molecule and 98% of small-molecule drugs entering the central nervous system [1–4]. Secondly, at the later stage of glioma, the blood–brain tumor barrier (BBTB) starts to form [5–7]. As most anti-tumor drugs are highly toxic to normal brain tissue, it is more important for drugs to accumulate in the glioma foci specifically after being transported across the blood–brain barrier. Finally, when drug delivery systems reach the glioma regions, most of the drugs are prevented from entering the brain tumor core due to several physiologic barriers such as high cell density and increased interstitial pressure, which also influences the therapeutic efficacy

[8,9]. Thus, researchers utilized various methods to conquer these barriers described above and achieved efficient glioma treatment. Since brain capillary endothelial cells express numerous different receptors, receptor-mediated transcytosis (RMT) is considered as one of the most common strategies among all the methods [10,11]. RMT provides a selective means for active BBB transporting and has been extensively studied for brain targeting [12–16]. However, specific ligands only have high affinity for targeted receptors and are usually not efficient enough to enhance endocytosis or solid tumor penetration [10,17,18]. On the other hand, cell penetrating peptides (CPP), a class of diverse short peptides widely used for siRNA, proteins and small molecular drugs delivery, also have the ability to carry drugs to penetrate BBB efficiently [19,20]. Nevertheless, because of their non-specific affinity to different cells, CPP-mediated brain delivery systems showed high drug distribution in the whole brain *in vivo* after systemic administration [21,22], and this property would lead to unwanted toxicity to normal brain tissues.

Thus, to overcome the impediments of both CPP and specific ligands, it is important to add a selective domain to CPP or enhance the penetrating capability of specific ligands. On this basis, a

\* Corresponding author. Tel./fax: +86 28 85502532.

E-mail addresses: [qinhe@scu.edu.cn](mailto:qinhe@scu.edu.cn), [qinhe317@126.com](mailto:qinhe317@126.com) (Q. He).

tandem peptide with multi functions was designed here. This kind of tandem peptide was consisted of a specific peptide in the front position and a cell penetrating peptide in the backend so that it could possess both specific targeting and high penetrating ability. Recently these multifunctional ligands have been drawing great attention [23–26]. Ren et al. [23] designed and screened a library of tandem peptides by linking LyP-1, a constant tumor penetrating domain, to a series of CPPs as vectors for siRNA delivery *in vitro*. However, current researches mainly focused on studying the structure–activity relationship of different kinds of CPP-linked tandem peptides and are lack of *in vivo* results. These tandem peptides have not been reported being used as a targeting ligand to modify nano carriers neither. In this study, cyclic RGD [c(RGDfK)] and octa-arginine (R8) were chosen as the specific and CPP domain of the tandem peptide respectively. RGD peptide is widely used as a specific ligand for integrin  $\alpha_v\beta_3$  family, which is over expressed on angiogenic endothelial cells and most malignant tumor cells including glioma cells, melanoma cells, oophoroma cells and so on [27–29]. It is also reported that cyclic RGD peptide has 1000 times greater binding affinity compared to linear RGD peptide. The advantages of cyclic RGD peptide in glioma targeting drug delivery systems were already confirmed [9,30,31]. Here cyclic RGD peptide was conjugated to R8 through amide bond to obtain a tandem peptide R8-RGD [RRRRRRRR-c(RGDfK), the branch of lysine is conjugated to octa-arginine]. We used liposomes as drug carriers and paclitaxel as a model drug. Since  $\alpha_v\beta_3$  integrin receptor is over expressed on both brain capillary endothelial cells and glioma cells [32], R8-RGD can be used as a promising multifunctional ligand for BBB transporting, glioma targeting and tumor penetrating. When RGD in the front position recognize  $\alpha_v\beta_3$  integrin receptor on brain capillary endothelial cells, R8 in the backend can exert the high penetrating capability to mediate drug delivery systems to transport across BBB. Then R8-RGD modified liposomes can also be specifically targeted to the brain tumor region and finally delivered

into the glioma core on the synergetic effect of R8 and RGD (as illustrated in Fig. 1). We evaluated the cellular uptake efficiency, the BBB penetrating and brain tumor penetrating capability of R8-RGD peptide *in vitro*, studied the brain targeting properties *in vivo* systemically, and investigated the therapeutic efficacy of paclitaxel loaded R8-RGD modified liposomes.

## 2. Materials and methods

### 2.1. Materials

Cyclic RGD peptide with a terminal cysteine [Cys-c(RGDfK), cysteine conjugated to the branch of lysine] and R8-RGD peptide with a terminal cysteine [Cys-RRRRRRRR-c(RGDfK), cysteine modified octa-arginine conjugated to the branch of lysine] were synthesized according to the standard solid phase peptide synthesis by Chinapeptides Co. Ltd. (Shanghai, China). R8 peptide with a terminal cysteine (Cys-RRRRRRRR) was synthesized according to the standard solid phase peptide synthesis by Chengdu Kai Jie Bio-pharmaceutical Co. Ltd. (Chengdu, China). Soybean phospholipids (SPC) were purchased from Shanghai Taiwei Chemical Company (Shanghai, China). Cholesterol was purchased from Chengdu Kelong Chemical Company (Chengdu, China). DSPE-PEG<sub>2000</sub>, DSPE-PEG<sub>2000</sub>-Mal and 1, 2-dioleoyl-sn-glycero-3-phosphoethanolamine-N-(carboxyfluorescein) (CFPE) were purchased from Avanti Polar Lipids (USA). Paclitaxel (PTX) was purchased from AP Pharmaceutical Co. Ltd. (Chongqing, China). 4'-6-diamidino-2-pheylindole (DAPI) and 3-(4, 5-Dimethylthiazol- 2-yl)-2, 5-diphenyltetrazolium bromide (MTT) were purchased from Beyotime Institute Biotechnology (Haimen, China). Rabbit anti-mouse  $\beta$ -actin and  $\beta_3$  integrin primary antibodies were purchased from Epitomics, Abcam (California, USA). Horseradish peroxidase (HRP) -labeled goat anti-rabbit secondary antibodies was purchased from ZSGB-BIO (Beijing, China). Poly-lysine, sodium azide, amiloride, chlorpromazine and filipin were obtained from Sigma–Aldrich (St. Louis, MO, USA). Lyso-tracker™ was purchased from Invitrogen (Carlsbad, CA, USA). 1, 10-Dioctadecyl-3, 3, 30, 30-tetramethylindotricarbocya-nine iodide (DiR) and 1, 10-dioctadecyl-3, 3, 30, 30-tetramethylindodicarbocyanine, 4-chlorobenzenesulfonate salt (DiD) were purchased from Biotium (USA). Annexin V-FITC/PI apoptosis detection kit was obtained from KeyGEN Biotech (China). Millicell Hanging Cell Culture Inserts were purchased from Millipore (USA). Plastic cell culture dishes and plates were purchased from Wuxi NEST Biotechnology Co. (Wuxi, China). The other chemicals were obtained from commercial sources.

Balb/c mice were purchased from West China animal center of Sichuan University (Sichuan, China). All animal procedures for this study were approved by the Experiment Animal Administrative Committee of Sichuan University.

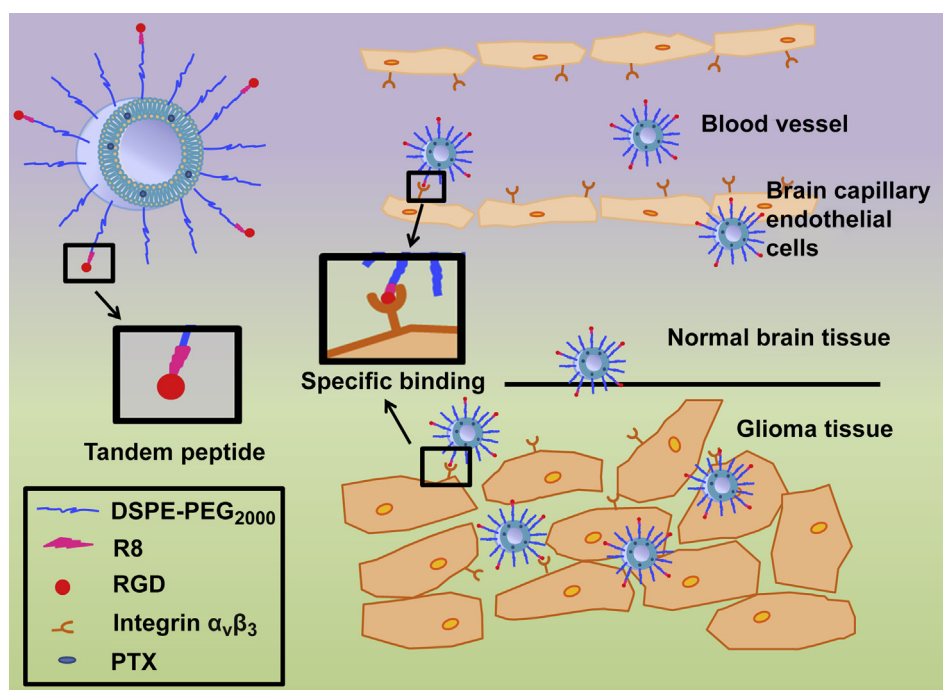


**Fig. 1.** Schematic illustration of PTX-loaded R8-RGD modified liposomes (PTX-R8-RGD-lipo). Liposomes could specifically bind to integrin  $\alpha_v\beta_3$  receptors expressed on the brain capillary endothelial cells and transport across the BBB through a synergetic effect. Then the liposomes could accumulate in the glioma tissue selectively, penetrate into the core region of tumor and release drugs.

## 2.2. Synthesis of different materials

DSPE-PEG<sub>2000</sub>-R8-RGD, DSPE-PEG<sub>2000</sub>-R8 and DSPE-PEG<sub>2000</sub>-RGD were synthesized by conjugating the cysteine residue of these three peptides to DSPE-PEG<sub>2000</sub>-Mal, respectively. Briefly, DSPE-PEG<sub>2000</sub>-Mal and Cys-R8-RGD (molar ratio 1:1.5) were mixed in chloroform/methanol (*v/v* = 2:1), and triethylamine was employed as a catalyst. Then the mixture was gently stirring for 24 h in darkness at room temperature. After thin layer chromatography showed the disappearance of DSPE-PEG<sub>2000</sub>-Mal, the mixture was evaporated by rotary evaporation under vacuum. The residue was redissolved by chloroform and the solution was filtered to purify production. Then the filtrate was evaporated again by rotary evaporation and the production DSPE-PEG<sub>2000</sub>-R8-RGD was stored under -20 °C. DSPE-PEG<sub>2000</sub>-R8 and DSPE-PEG<sub>2000</sub>-RGD were synthesized by similar methods with the Cys-R8-RGD being replaced by Cys-R8 or Cys-RGD. The existence of these three products was confirmed by MALDI-TOF mass spectrometry (MALDI-TOF MS).

## 2.3. Preparation and characterization of liposomes

Liposomes were prepared by thin film hydration method. Lipid compositions of the prepared liposomes were as follows: (1) conventional PEGylated liposomes (PEG-lipo), SPC/cholesterol/DSPE-PEG<sub>2000</sub> (molar ratio = 62:33:5); (2) R8-RGD modified liposomes (R8-RGD-lipo), SPC/cholesterol/DSPE-PEG<sub>2000</sub>/DSPE-PEG<sub>2000</sub>-R8-RGD (molar ratio = 62:33:4.2:0.8); (3) R8 modified liposomes (R8-lipo), SPC/cholesterol/DSPE-PEG<sub>2000</sub>/DSPE-PEG<sub>2000</sub>-R8 (molar ratio = 62:33:4.2:0.8); (4) RGD modified liposomes (RGD-lipo), SPC/cholesterol/DSPE-PEG<sub>2000</sub>/DSPE-PEG<sub>2000</sub>-RGD (molar ratio = 62:33:4.2:0.8). All lipid materials were dissolved in chloroform, and then the organic solvent was removed by rotary evaporation to form a lipid film. After kept in vacuum overnight, the obtained film was hydrated in PBS (pH 7.4) for 20 min at 37 °C. Then it was further intermittently sonicated by a probe sonicator at 80 W for 80 s to form liposomes.

CFPE-labeled, DiD-loaded, DiR-loaded, and PTX-loaded liposomes were prepared with appropriate amount of CFPE, DiD, DiR and PTX added to the lipid organic solution, respectively. The entrapment efficiency of PTX was determined by high performance liquid chromatography (Agilent 1200, USA). The mean size and zeta-potential of PEG-lipo, R8-RGD-lipo, R8-lipo and RGD-lipo were detected by Malvern Zetasizer Nano ZS90 (Malvern Instruments Ltd., UK). Transmission electron microscope (TEM) (JEM-100CX, JEOL, Japan) was used for the morphological examination of R8-RGD-lipo following negative staining with sodium phosphotungstate solution.

Turbidity variations of liposomes were monitored in 50% fetal bovine serum (FBS) to evaluate the serum stability of liposomes. In brief, liposomes were mixed with FBS (*v/v* = 1:1), and the mixture was then incubated at 37 °C for 48 h. The transmittance of the mixture was measured at predetermined time points (0 h, 1 h, 2 h, 4 h, 8 h, 12 h, 24 h and 48 h) at 750 nm by a microplate reader (Thermo Scientific Varioskan Flash, USA).

*In vitro* PTX release study was performed with a dialysis method. PBS (pH 7.4) containing 0.1% (*v/v*) Tween 80 was used as the release media. PTX-loaded liposomes or free PTX were placed into dialysis tubes (MWCO = 8000 Da) and tightly sealed. The dialysis tubes were added into 50 ml release media and incubated at 37 °C with gently oscillating for 48 h. At predetermined time points, 0.1 ml release media was sampled and replaced with equal volume of fresh release media. The samples were then analyzed by HPLC to determine the concentrations of PTX.

## 2.4. Cell culture

Murine glioma cells (C6) and murine melanoma cells (B16) were cultured in RPMI-1640 medium at 37 °C in a 5% CO<sub>2</sub> humidified environment incubator (Thermo Scientific, USA), human cervical carcinoma cells (Hela) and murine brain endothelial cells (bEnd.3) were cultured in DMEM medium under the same condition. Both medium contained 10% FBS, 100 U/ml penicillin and 100 µg/ml streptomycin.

## 2.5. Integrin $\alpha_v\beta_3$ expression level

The expression level of integrin  $\alpha_v\beta_3$  on murine B16 cells, bEnd.3 cells and C6 cells was measured by western blot studies. Approximately  $3 \times 10^6$  cells were homogenized with cell lysis buffer containing protease inhibitors. Then appropriate total protein samples of different cells were resolved on 10% SDS-PAGE. The gels were transferred to polyvinylidene difluoride membranes, and incubated with Rabbit anti-mouse  $\beta$ -actin or  $\beta_3$  integrin primary antibodies. Then the membranes were incubated with HRP-labeled goat anti-rabbit secondary antibodies and detected by Immobilon Western HRP Substrate (Millipore, USA) on a Bio-Rad ChemiDoc MP System (Bio-Rad Laboratories, USA). As for the human cells, the expression level of integrin  $\alpha_v\beta_3$  was measured by a flow cytometer. Briefly, Hela cells were incubated with FITC labeled anti-human integrin  $\alpha_v\beta_3$  antibody for 20 min at 4 °C, and then the fluorescent intensity of antibody treated Hela cells was measured by a flow cytometer (Cytomics FC 500, Beckman Coulter, USA).

## 2.6. Cellular uptake study

### 2.6.1. Cellular uptake on different cells

C6 cells, bEnd.3 cells and Hela cells were plated in six-well plates at a density of  $5 \times 10^5$  cells per well and cultured for 24 h. CFPE-labeled liposomes were prepared as described above. Different formulations of liposomes were added into the plates at a final CFPE concentration of 1.5 µg/ml. After incubation for 4 h at 37 °C, the cells were washed three times with cold PBS, trypsinized, and finally resuspended in 0.5 ml PBS. The fluorescent intensity of cells treated with different liposomes was measured by a flow cytometer (Cytomics FC 500, Beckman Coulter, USA).

For qualitative experiments, C6 cells, bEnd.3 cells and Hela cells were plated at a density of  $1 \times 10^5$  cells per well on gelatin-coated cover slips in six-well plates and cultured for 24 h. CFPE-labeled liposomes were added into the plates as described in the quantitative studies. After 4 h incubation, the cells were washed with cold PBS for three times and fixed with 4% paraformaldehyde for 30 min at room temperature. Then DAPI was added for 5 min for nuclei staining. Finally, the cells were imaged by a confocal microscope (FV1000, Olympus, USA).

### 2.6.2. Uptake mechanism study

In order to study the uptake mechanism of R8-RGD-lipo, C6 cells were pre-incubated with various endocytosis inhibitors including poly-lysine (400 µg/ml), sodium azide (6.51 mg/ml), amiloride (1.48 mg/ml), chlorpromazine (10 µg/ml) and filipin (10 µg/ml), meanwhile the inhibition of free RGD peptide (100 µg/ml) and the effect of temperature were also studied. After 30 min pre-incubation with the inhibitors above, CFPE-labeled R8-RGD modified liposomes were added for further 4 h incubation. Then the cells were treated as described in 2.6.1 and the fluorescent intensity was determined by a flow cytometer (Cytomics FC 500, Beckman Coulter, USA).

### 2.6.3. Co-localization of liposomes and lysosome

For the intracellular location studies of different liposomes, lysosomes were staining to co-localize liposomes. Briefly, after 4 h incubation of CFPE-labeled liposomes, C6 cells were washed with serum free medium and treated with Lyso-Tracker (50 nM) for 1 h. Then the cells were treated as described in 2.6.1, and a confocal microscope (FV1000, Olympus, USA) was used to observe the cells.

## 2.7. C6 tumor spheroid uptake

Avascular C6 tumor spheroids were established as follows: first, a 96-well plate was coated with 2% (*w/v*) low melting point agarose to prevent cell adhesion, then  $5 \times 10^3$  C6 cells were plated on the pre-coated 96-well plate and incubated for 7 days. The uniform and compact spheroids were selected and incubated with CFPE-labeled liposomes for 4 h, then the spheroids were washed with cold PBS for three times and subjected to confocal microscopy analysis (TCS SP5 AOBs confocal microscopy system, Leica, Germany).

## 2.8. BBB model study *in vitro*

### 2.8.1. BBB model permeability study

Millicell Hanging Cell Culture Inserts were used to establish BBB model *in vitro*. In brief, bEnd.3 cells were plated into the 6-well cell culture inserts at a density of  $1 \times 10^6$  cells per well, and cultured for about one week. Then the transendothelial electric resistance (TEER) of the BBB model was measured by Millicell ERS (Millipore, USA). Only the bEnd.3 monolayers with TEER over 200 Ω were used for further studies. On the other hand, C6 cells were plated in another 6-well plate. Then the cell culture inserts with bEnd.3 monolayers were transferred to the plates containing C6 cells and co-cultured for another day. CFPE-labeled liposomes were added in the cell culture inserts (donor chamber). After 8 h incubation, bEnd.3 cells on the cell culture inserts and C6 cells on the plates of the substratum (acceptor chamber) were washed with cold PBS for three times, trypsinized, and finally resuspended in 0.5 ml PBS, respectively. Then the fluorescent intensity of both cells was measured by a flow cytometer (Cytomics FC 500, Beckman Coulter, USA). On the other hand, C6 cells on the plates of the substratum were also treated as described in 2.6.1 and a confocal microscope was used to observe the cells.

The tumor spheroid penetration ability of liposomes after permeating BBB model *in vitro* was studied as well. BBB model was established as above with 6-well inserts being replaced by 24-well inserts and C6 spheroids were prepared as described in 2.7. Then C6 spheroids were transferred into a 24-well plate and cell culture inserts with bEnd.3 monolayer were placed above the spheroids. CFPE-labeled liposomes were added into the donor chamber for 8 h incubation, then C6 spheroids were washed with cold PBS for three times and subjected to confocal microscopy analysis (TCS SP5 AOBs confocal microscopy system, Leica, Germany).

### 2.8.2. Confocal microscope study of bEnd.3 monolayer

To obtain images of bEnd.3 cells monolayer grown on Millicell Hanging Cell Culture Inserts, the poly-carbonate membranes with bEnd.3 cells monolayers on them was cut off from the inserts after 8 h incubation with CFPE-labeled liposomes.

The membranes were then washed with cold PBS for three times, fixed with 4% paraformaldehyde and stained with DAPI. The samples were imaged using a confocal microscope (FV1000, Olympus, USA). Serial pictures along the  $x-z$  axis were captured and the bEnd.3 monolayers were observed from both  $x-y$  plane and  $x-z$  plane.

### 2.9. Cytotoxicity study *in vitro*

The cytotoxicity of PTX-loaded liposomes was measured with MTT assay. C6 cells were plated in 96-well plates at a density of  $2 \times 10^3$  cells per well and cultured for 24 h. PTX-loaded liposomes and free-PTX were diluted to predetermined concentrations with PBS, and added into each well for 24 h incubation. The final concentrations of PTX were in the range of 0.1–20  $\mu\text{g/ml}$ . Blank liposomes and the solvent of free PTX (ethanol-cremophor ELP 35 mixture,  $v/v = 1:1$ ) were added at the same concentration of PTX-loaded liposomes as well. Then 20  $\mu\text{l}$  MTT (5 mg/ml in PBS) was added into each well and incubated for 4 h under 37 °C. Finally the medium was removed and replaced by 150  $\mu\text{l}$  dimethyl sulfoxide. Then the absorbance was measured by a microplate reader (Thermo Scientific Varioskan Flash, USA) at 570 nm. The cells treated with medium were evaluated as controls. Cell viability was calculated by the following formula: cell viability (%) =  $A_{\text{treated}}/A_{\text{control}} \times 100$ , in which  $A_{\text{treated}}$  and  $A_{\text{control}}$  represented the absorbance of treated cells and control cells, respectively.

### 2.10. Apoptosis study *in vitro*

To evaluate the cell apoptosis induced by PTX-loaded liposomes, C6 cells were treated with PTX-loaded liposomes (PTX concentration of 0.5  $\mu\text{g/ml}$ ) for 24 h under 37 °C. Free PTX group was used as control. Cells were harvested, washed three times with cold PBS and resuspended in 500  $\mu\text{l}$  binding buffer. Then 5  $\mu\text{l}$  Annexin V-FITC and 5  $\mu\text{l}$  PI were added and incubated with the cells for 15 min in the dark. Finally, the stained cells were analyzed by a flow cytometer (Cytomics FC 500, Beckman Coulter, USA).

### 2.11. *In vivo* experiments

#### 2.11.1. Glioma model establishment

Balb/c mice were anesthetized with 5% chloral hydrate and placed on a stereotaxic apparatus. C6 cells ( $1 \times 10^6$  cells/5  $\mu\text{l}$ ) were injected into the right brain of each Balb/c mouse. These mice were raised under standard condition for 1 week and used for subsequent experiments.

#### 2.11.2. *In vivo* imaging

DiR-loaded liposomes were prepared as described above and were intravenously injected to the glioma bearing mice at a dose of 200  $\mu\text{g}$  DiR/kg. The mice were imaged with IVI Spectrum system (Caliper, Hopkington, MA, USA) at 1 h, 4 h, 8 h and 24 h after injection. Then the mice were sacrificed after heart perfusion with PBS at these pre-determined time points. Brains, hearts, livers, spleens, lungs and kidneys were collected. All the organs were imaged with IVI Spectrum system (Caliper, Hopkington, MA, USA) as well.

#### 2.11.3. Glioma distribution

Glioma bearing mice were intravenously injected with DiD-loaded liposomes at a dose of 500  $\mu\text{g}$  DiD/kg. Eight hours later, the mice were sacrificed after heart perfusion with saline and 4% paraformaldehyde. Brains were collected and the glioma domains were sectioned at a thickness of 10  $\mu\text{m}$ . Then the sections were incubated with DAPI to stain nuclei. Finally, the sections were imaged by a laser scanning confocal microscope (FV1000, Olympus, USA).

#### 2.11.4. Anti-glioma efficacy

Sixty intracranial C6 glioma bearing Balb/c mice were divided into 6 groups randomly ( $n = 10$ ). The mice were intravenously injected with free PTX, PTX-PEG-lipo, PTX-R8-RGD-lipo, PTX-R8-lipo and PTX-RGD-lipo (PTX dose of 3 mg/kg) at 4, 6, 8, 10, 12 and 14 days after implantation. Saline group was used as negative control. The survival time of each group was recorded and analyzed.

### 2.12. Statistical analysis

All the data were presented as mean  $\pm$  standard deviation. Statistical comparisons were performed by analysis of variance (ANOVA) for multiple groups, and  $p$  value  $< 0.05$  and  $< 0.01$  were considered indications of statistical difference and statistically significant difference respectively.

## 3. Results and discussions

### 3.1. Synthesis of materials

We conjugated the tandem peptide R8-RGD to the distal end of DSPE-PEG<sub>2000</sub>-Mal by the Michael addition of cysteine residue and maleimide. In order to verify the synergistic effect of the tandem

peptide, the cell penetrating peptide R8 and the specific ligand peptide RGD were used as control groups, and conjugated to DSPE-PEG<sub>2000</sub>-Mal by the same method. The results of mass spectrometry confirmed the formation of all the three products, which were DSPE-PEG<sub>2000</sub>-R8-RGD (MW observed = 4892 Da, MW calculated = 4898 Da), DSPE-PEG<sub>2000</sub>-R8 (MW observed = 4295 Da, MW calculated = 4312 Da) and DSPE-PEG<sub>2000</sub>-RGD (MW observed = 3759 Da, MW calculated = 3748 Da) (See [Supplementary Information Fig. S1](#)).

### 3.2. Characterizations of liposomes

Proper sizes and uniform distribution of nanoparticles were required for both BBB permeation and brain tumor targeting [33]. The particle sizes and zeta potentials of different liposomes in this study were listed in [Table 1](#). For all the liposomes with different modifications, with or without PTX, the average particle sizes were less than 110 nm and PDI were about 0.2, implying uniform distribution of all groups of liposomes. The sizes of PTX-loaded liposomes increased a little compared to the blank liposomes. The zeta potentials of PEG-lipo and RGD-lipo were about  $-7$  mV. When modified with R8, the liposomes became less negative charged (approximately  $-4$  mV) because of the electropositivity of arginine. And the zeta potential of R8-RGD modified liposomes was between PEG-lipo and R8-lipo, which implied that the positive charge of R8 was partly shielded by the RGD domain. The entrapment efficiencies of all different kinds of PTX-loaded liposomes were about 90%.

[Fig. 2A](#) showed the schematic diagram of the PTX-R8-RGD-lipo. The size and zeta potential distribution graphs of PTX-R8-RGD-lipo were shown in [Fig. 2B](#) and C, and PTX-R8-RGD-lipo exhibited spherical shape under TEM ([Fig. 2D](#)).

Transmittance of different liposomes were monitored in the presence of 50% FBS. As shown in [Fig. 2E](#), the transmittance of all the liposomes were above 90% and hardly changed after 48 h incubation with 50% FBS. This stability study of liposomes also laid foundation for the further *in vivo* experiments.

### 3.3. *In vitro* PTX release study

PTX release properties were evaluated in PBS containing 0.1% Tween 80. As shown in [Fig. 3](#), free PTX exhibited a rapid release, with over 80% of the drug released into the media within 6 h incubation. On the other hand, PTX-loaded liposomes achieved sustained release behaviors that the cumulative PTX release of drug loaded liposomes was less than 60% after 48 h incubation in PBS. No significant difference on release properties was observed among PEG-lipo, R8-RGD-lipo, R8-lipo and RGD-lipo, and none of these four kinds of PTX-loaded liposomes displayed burst initial release patterns.

**Table 1**

Particle sizes and zeta potentials of different liposomes and the PTX entrapment efficiency of PTX-loaded liposomes ( $n = 3$ , mean  $\pm$  SD).

	Size (nm)	PDI	Zeta potential (mV)	Entrapment efficiency (%)
PEG-lipo	98.12 $\pm$ 1.2	0.186 $\pm$ 0.013	-6.86 $\pm$ 0.71	-
R8-RGD-lipo	102.4 $\pm$ 1.8	0.211 $\pm$ 0.015	-5.97 $\pm$ 0.45	-
R8-lipo	100.1 $\pm$ 2.5	0.212 $\pm$ 0.016	-3.78 $\pm$ 0.34	-
RGD-lipo	101.9 $\pm$ 2.9	0.224 $\pm$ 0.038	-7.54 $\pm$ 0.25	-
PTX-PEG-lipo	106.2 $\pm$ 2.6	0.198 $\pm$ 0.022	-7.79 $\pm$ 0.33	90.94 $\pm$ 6.92
PTX-R8-RGD-lipo	105.9 $\pm$ 0.7	0.186 $\pm$ 0.027	-4.95 $\pm$ 0.59	92.50 $\pm$ 5.06
PTX-R8-lipo	105.5 $\pm$ 2.5	0.197 $\pm$ 0.011	-4.07 $\pm$ 0.20	89.58 $\pm$ 3.86
PTX-RGD-lipo	105.2 $\pm$ 1.4	0.187 $\pm$ 0.007	-7.14 $\pm$ 0.19	94.87 $\pm$ 1.20

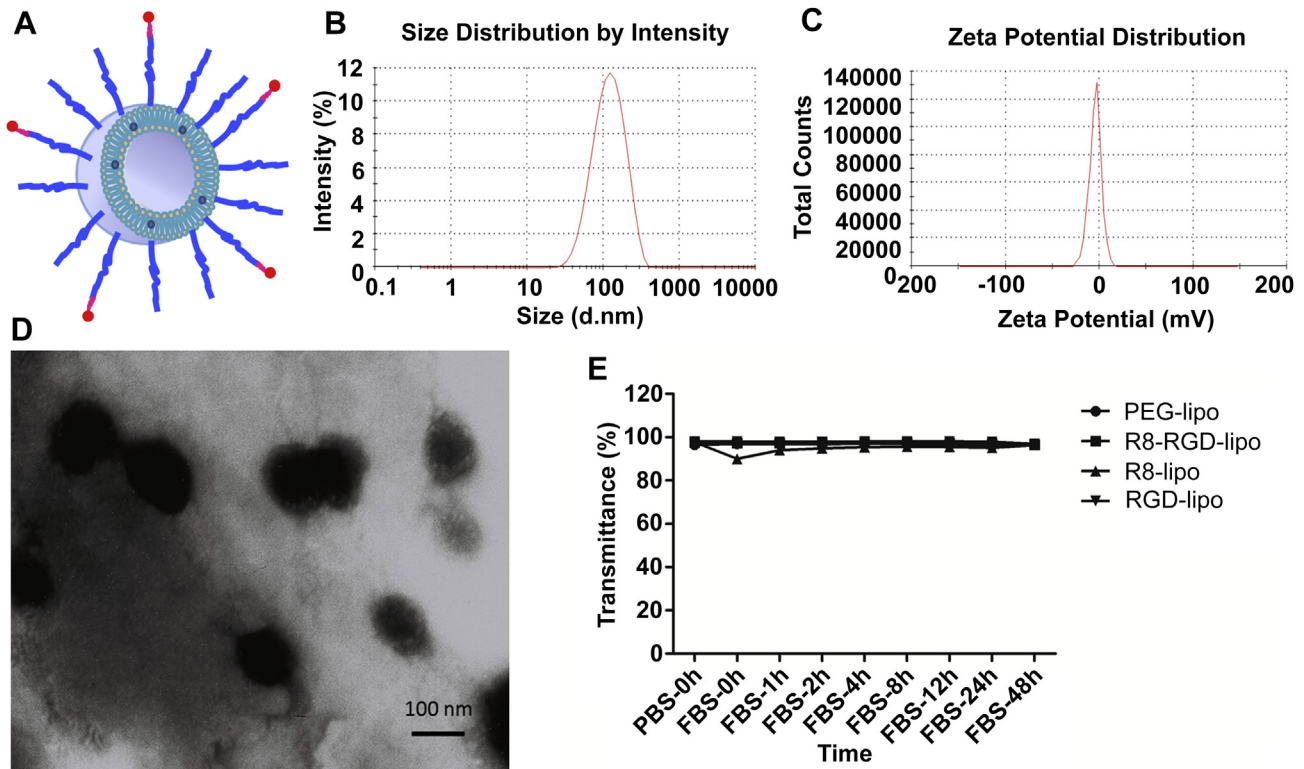


**Fig. 2.** Characterization of liposomes. (A) Schematic of PTX-R8-RGD-lipo. (B) Size distribution graph of PTX-R8-RGD-lipo. (C) Zeta potential distribution graph of PTX-R8-RGD-lipo. (D) Transmission electron microscopy images of PTX-R8-RGD-lipo. (E) The variations of transmittance of different modified liposomes in 50% FBS ( $n = 3$ , mean  $\pm$  SD).

### 3.4. Integrin $\alpha_v\beta_3$ expression level

High expression of integrin  $\alpha_v\beta_3$  on both brain capillary endothelial cells and glioma cells is a prerequisite of this system. In this section, receptor expression levels on the targeted cells were monitored by western blot studies. Anti-mouse integrin  $\beta_3$  antibodies were used to immunoblot the cells. The results showed that both bEnd.3 cells and C6 cells demonstrated high expression levels of integrin  $\alpha_v\beta_3$  (Fig. 4E), which confirmed that the tandem peptide modified liposomes might have the ability to target both blood–brain barrier and glioma as we assumed initially. The receptor expression levels were also tested on B16 cells (murine melanoma cells), a kind of reported integrin-overexpressed cells [34,35].

Integrin  $\alpha_v\beta_3$  receptors were also found highly expressed on B16 cells. On the other hand, a flow cytometer was used to detect the expression level of integrin  $\alpha_v\beta_3$  receptors on HeLa cells (See Supplementary Information Fig. S2), which were reported expressing fewer integrin receptors [36], results showed that the fluorescence intensity of HeLa cells treated with FITC-labeled anti-human integrin  $\alpha_v\beta_3$  antibody hardly increased compared to the non-treated cells, indicating a low integrin  $\alpha_v\beta_3$  expression level of HeLa cells.

### 3.5. Cellular uptake study

The bEnd.3 cells were murine brain endothelial cells exhibiting endothelial properties. Thus this cell line was widely used as a model for mimicking brain capillary endothelial cells and evaluating the BBB penetrating capability *in vitro* [37,38]. As the Integrin  $\alpha_v\beta_3$  receptors were certified to be expressed on both bEnd.3 cells and C6 cells, the cellular uptake of different modified liposomes was studied. Unmodified PEGylated liposomes were used as negative control. As flow cytometry results showed (Fig. 4C), liposomes modified with RGD peptide increased the cellular uptake on both cells compared to the negative control. However, the fluorescence intensity of RGD-lipo treated cells was far lower than R8-lipo group and R8-RGD-lipo group. This was because specific receptor targeting peptides like RGD, also called homing peptides (HP), had high affinity to their homologous receptors but relatively lower internalization properties [39]. Therefore specific ligands mainly delivered their cargo to the cell surface instead of penetrating the cell membranes. R8-modified liposomes unsurprisingly displayed higher uptake level than PEG-lipo, as CPP had already proved their ability to deliver cargo into cells in many reports [40–43]. However, as for the tandem peptide, R8-RGD modified

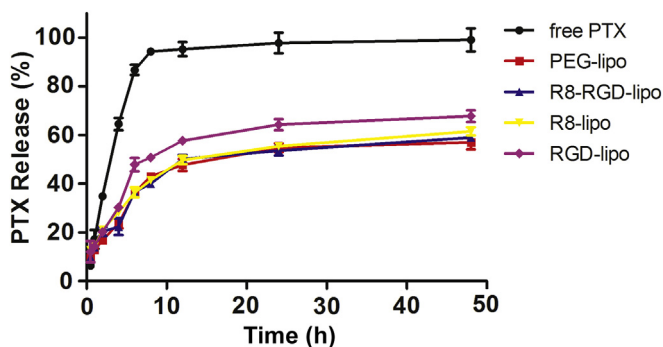


**Fig. 3.** The PTX release profiles of free PTX, PEG-lipo, R8-RGD-lipo, R8-lipo and RGD-lipo in PBS (pH 7.4) containing 0.1% Tween 80 over 48 h ( $n = 3$ , mean  $\pm$  SD).

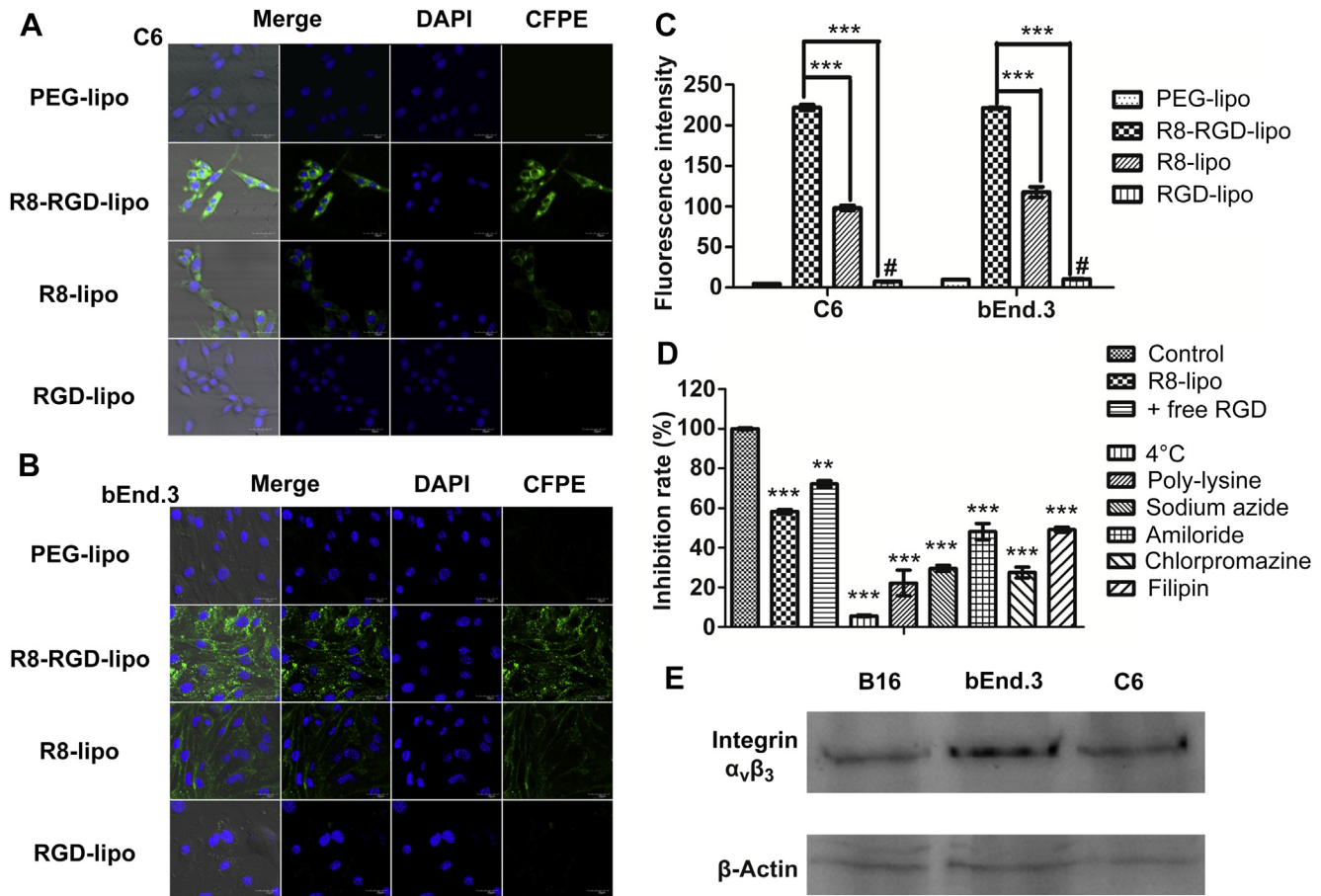


**Fig. 4.** Confocal images of cellular uptake of liposomes on C6 cells (A) and bEnd.3 cells (B) 4 h after liposomal treatment. (C) Cellular uptake of CFPE-labeled liposomes on C6 cells and bEnd.3 cells measured by a flow cytometer ( $n = 3$ , mean  $\pm$  SD), \*\*\*indicates statistically significant difference ( $p < 0.001$ ), #represents  $p < 0.05$  versus PEG-lipo group. (D) Uptake mechanism study of R8-RGD-lipo on C6 cells ( $n = 3$ , mean  $\pm$  SD), \*\* and \*\*\* represent  $p < 0.01$  and  $p < 0.001$  versus control group. (E) Expression level of integrin  $\alpha_v\beta_3$  on different murine cells.

liposomes showed the highest cellular uptake level on both bEnd.3 cells and C6 cells, about 2 times higher than R8-lipo and nearly 30 times higher than RGD-lipo. Similar results were obtained from confocal images (Fig. 4A and B). These data demonstrated that the tandem peptide R8-RGD not only combined the transcytosis capabilities of R8 and RGD themselves, but also exerted a synergetic effect. On the other hand, cellular uptake of these four kinds of liposomes was also measured on HeLa cells, which were proved to possess a lower integrin expression level. No significant increase was observed compared R8-RGD-lipo to R8-lipo (See Supplementary Information Fig. S2), confirming the specific targeting ability of R8-RGD peptide. In addition, as shown in the confocal images (Fig. 4A and B), R8 modified liposomes mostly accumulated on the cell membranes instead of in the cytoplasm on both cells, which was owing to the adsorption of positive charged R8 and negative charged cell membranes. However, when RGD was conjugated to R8, the positive charge of arginine was partially shielded and stronger green fluorescence was observed in the cytoplasm. This phenomenon also signified the superiority of the tandem peptide.

In order to study the uptake mechanism of R8-RGD-lipo, a series of endocytosis inhibitors were pre-incubated with C6 cells and the inhibition rate was calculated to analyze the uptake mechanism [44,45]. Firstly, as shown in Fig. 4D, the cellular uptake of R8-RGD-lipo was significantly decreased in the presence of free RGD peptide. This further proved that the RGD domain of R8-RGD increased

the cellular internalization by specifically binding to integrin receptors expressed on C6 cells. When targeting sites were competitively bound by free RGD, the cellular uptake of R8-RGD-lipo decreased. But the receptor sites might not be occupied completely, so the cellular uptake level of free RGD added group was still a little higher than R8 modified liposomes. In addition, other inhibitors were used to study the uptake mechanism. Poly-lysine was used as positive charge inhibitor; 4 °C and sodium amide were selected to study the effect of energy; amiloride, chlorpromazine and filipin were chosen to block macropinocytosis, clathrin-mediated and caveolin-mediated endocytosis respectively. As the results showed, every inhibitor showed different levels of inhibition effects (Fig. 4D). Poly-lysine showed a significant inhibition of liposomal cellular uptake down to 22.2%, indicating that octa-arginine domain of R8-RGD enhanced cellular internalizing through positive charged mediated adsorption. 4 °C and sodium amide also displayed strong impact on cellular uptake (down to 5.6% and 29.6% respectively), showing energy-dependent properties of integrin receptor mediated endocytosis. Meanwhile, amiloride, chlorpromazine and filipin inhibited the cellular uptake of R8-RGD-lipo down to 48.2%, 27.5% and 49.1%, respectively. Specific internalization is commonly considered to be clathrin-mediated endocytosis pathway [46,47], but our system had a specific ligand domain and a CPP domain at the same time. Therefore the tandem peptide R8-RGD might enhance the cellular uptake through a comprehensive pathway.

Receptor-mediated endocytosis usually led to endosome formation [10,48], and therapeutic agents could possibly turn inactivated under the acid environment in endosomes. Therefore it is necessary for a drug delivery system to escape endosomes in order for the drug to be therapeutically active in the cytoplasm. On the other hand, researches proved that arginine-rich cell penetrating peptides could lead to endosome escape [49,50]. In this study we colocalized liposomes with late endosomes and lysosomes in order to estimate the endosome escaping ability of the tandem peptide R8-RGD. As Fig. 5 showed, late endosomes and lysosomes were dyed red in the presence of Lyso-Tracker while green fluorescence represented CFPE-liposomes. Only a few RGD modified liposomes entered the cells and almost entirely localized in lysosomes (pointed by white arrows). R8-lipo mostly adsorbed on the cell membrane (consistent with the cellular uptake images), but the majority of R8-lipo escaped from lysosomes successfully. In the R8-RGD-lipo group, only a small amount of liposomes were trapped in lysosomes, and large area of green fluorescence was seen diffusing in the cytoplasm. The results demonstrated that R8-RGD had the ability to escape endosomes, which exhibited the potential of R8-RGD to be further used in gene delivery systems.

### 3.6. C6 tumor spheroid uptake

For solid tumor, several physiologic barriers such as high cell density, increased interstitial pressure and absence of vascular existed [51], and cells in the core region of solid tumor were hypoxic and necrotic. Traditional drugs could hardly be delivered deeper into the necrotic regions and as a result these so-called “blind areas” would inevitably lead to tumor relapse [9,52,53].

Thus the capability of a drug delivery system to penetrate deeper into the core region of solid tumor was necessary. Three-dimensional tumor spheroids were prepared here to evaluate the solid tumor penetration ability of liposomes. Fig. 6 showed confocal laser scanning microscope images of C6 tumor spheroids 4 h after incubating with CFPE-labeled liposomes. R8-RGD-lipo displayed stronger green fluorescence at different depths of C6 tumor spheroids compared to other groups. It is confirmed that R8-RGD possessed stronger penetration ability through the synergetic effect of R8 and RGD, as we hypothesized.

### 3.7. BBB model study *in vitro*

The bEnd.3 cells were used to establish a BBB model *in vitro* [54]. In this study, bEnd.3 cells were plated in the Millicell Hanging Cell Culture Inserts to construct a monolayer. Both bEnd.3 cells on the transwell membrane from the donor chamber and C6 cells on the plate substratum from the acceptor chamber were collected, and the fluorescence intensity was measured by a flow cytometer. As shown in Fig. 7A, the cellular uptake results on bEnd.3 monolayer were similar to the uptake data on bEnd.3 cells in Fig. 4C, indicating that bEnd.3 monolayer on the Transwell membrane could internalize liposomes normally. However, as for the liposomal uptake on C6 cells after penetrating bEnd.3 monolayer, only R8-RGD-lipo displayed extremely higher fluorescence intensity on C6 cells than any other groups. Confocal images of C6 cells also confirmed these results (Fig. 7B). Green fluorescence signal of CFPE-labeled liposomes could hardly be observed except the R8-RGD-lipo group. As we proved in the cellular uptake study part, R8 modified liposomes mostly adsorbed on the cell membrane (Fig. 4A and B), thus R8-lipo might mainly stay on the

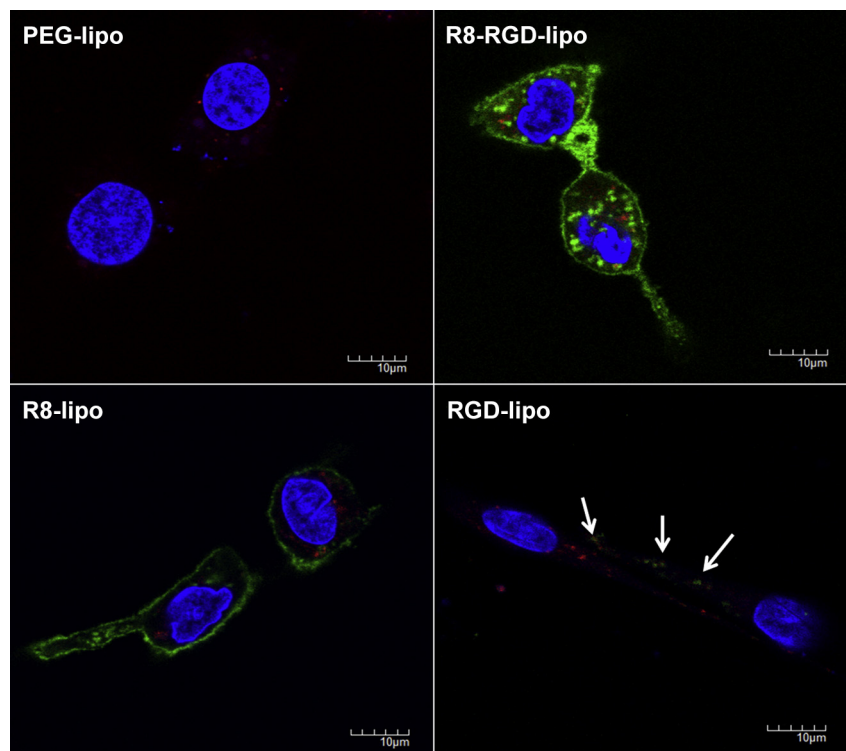


**Fig. 5.** Colocalization of CFPE-labeled liposomes (green) and lysosomes (red). Nuclei were stained with DAPI (blue). White arrow pointed to the colocalized yellow sites of liposomes and lysosomes. (For interpretation of the references to color in this figure legend, the reader is referred to the web version of this article.)

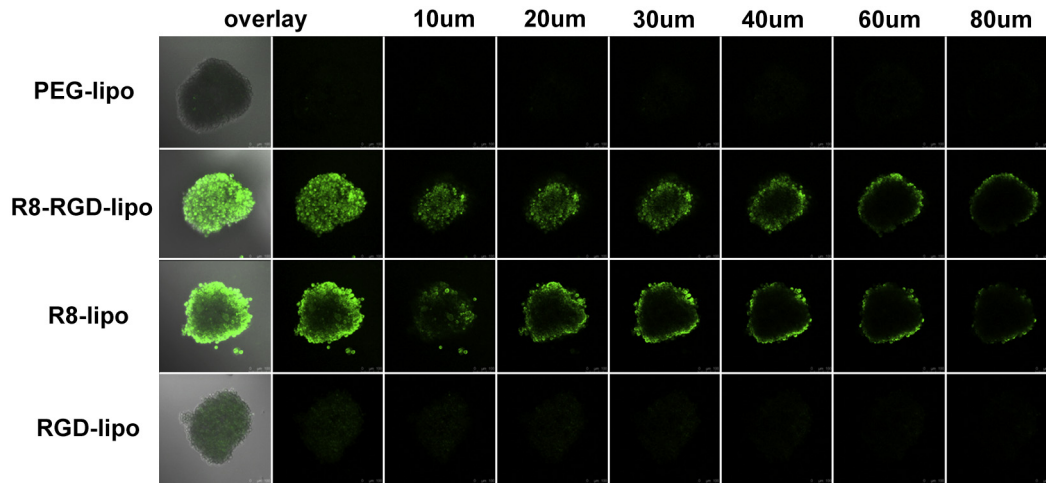


Fig. 6. CLSM images of C6 tumor spheroids uptake of CFPE-labeled liposomes within different depth.

monolayers instead of penetrating them. But R8-RGD-lipo could successfully transport across the bEnd.3 monolayer and be delivered to the C6 cells. Then we cut the transwell membranes and captured pictures along the x-z axis. As shown in Fig. 7C, x-y plane of the monolayer was shown in the top, and pictures in the bottom demonstrated the x-z plane, which showed the longitudinal section of the yellow line position in the homolog x-y plane. White arrows pointed to the transwell membrane. Strongest green

fluorescence was clearly observed transporting across the bEnd.3 monolayer in the R8-RGD-lipo group. On the other hand, the bEnd.3 monolayers were also co-cultured with C6 spheroids. The confocal images of C6 spheroids uptake in the presence of a bEnd.3 monolayer were shown in Fig. 8. R8-RGD-lipo group still exhibited the strongest fluorescence. To sum up, R8-RGD peptide displayed superior BBB transporting and tumor penetrating capabilities in the BBB model study.

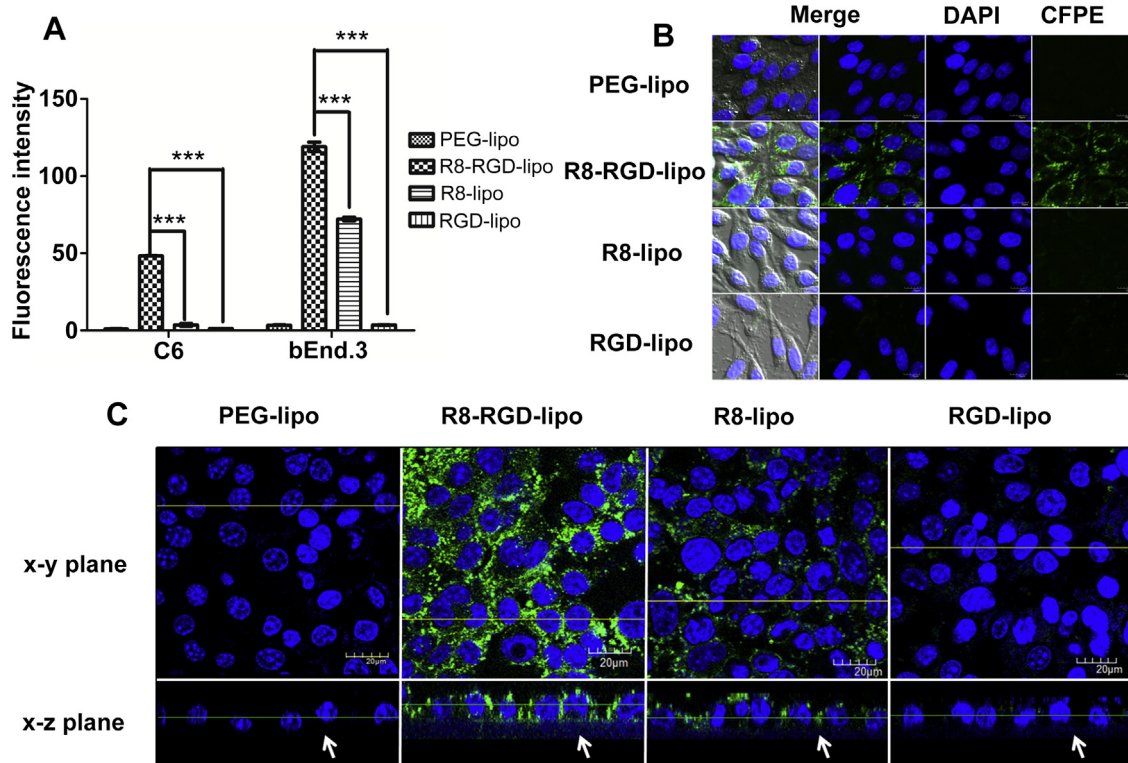


Fig. 7. The BBB model study. (A) Uptake of CFPE-labeled liposomes on C6 cells in the presence of BBB model and uptake on bEnd.3 cells on the transwell membrane measured by a flow cytometer ( $n = 3$ , mean  $\pm$  SD), \*\*\*indicates statistically significant difference ( $p < 0.001$ ). (B) Confocal images of the uptake of CFPE-labeled liposomes on C6 cells in the presence of bEnd.3 monolayers. (C) CLSM images of bEnd.3 cell monolayers grown on transwell membranes. Images were taken along the z-axis and shown in both x-y plane and x-z plane. The membranes were pointed by white arrows.

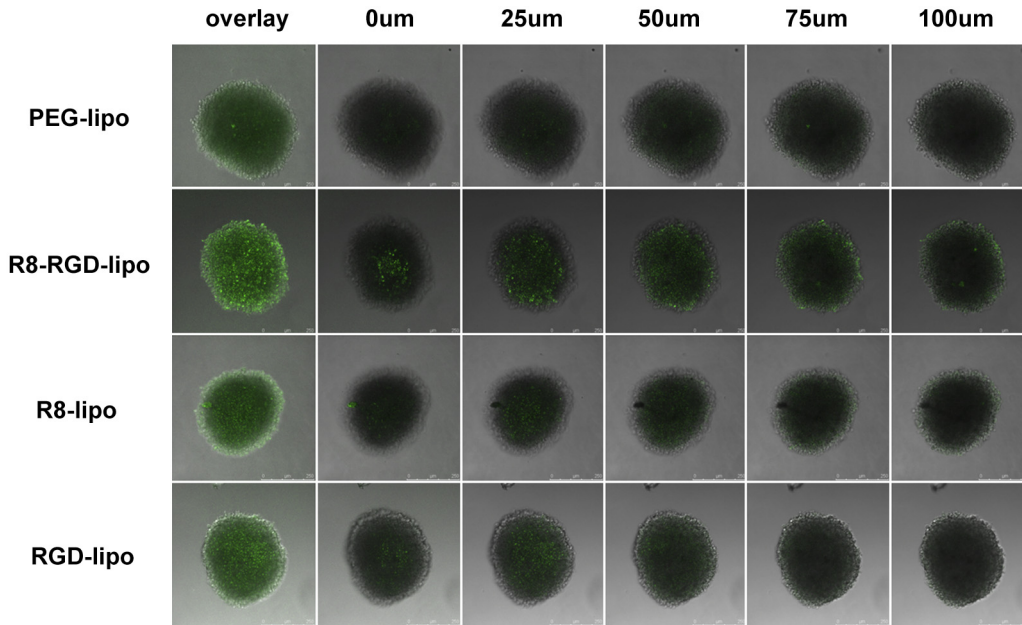


Fig. 8. CLSM images of C6 tumor spheroids uptake of CFPE-labeled liposomes in the presence of bEnd.3 monolayers within different depth.

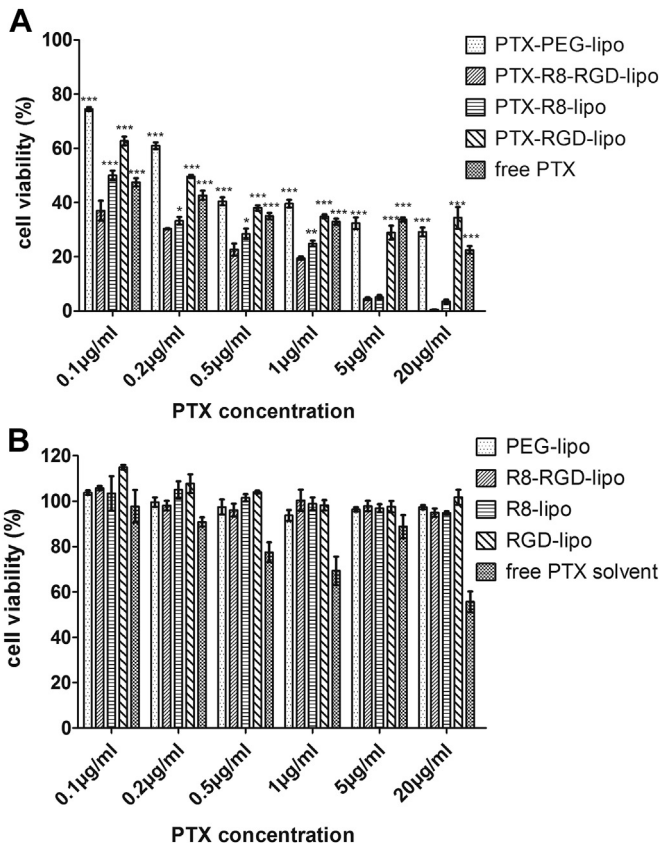


Fig. 9. (A) The cytotoxicity study of PTX-loaded liposomes and free PTX on C6 cells ( $n = 3$ , mean  $\pm$  SD), \*, \*\* and \*\*\* represent  $p < 0.05$ ,  $p < 0.01$  and  $p < 0.001$  versus PTX-R8-RGD-lipo group, respectively. (B) The cytotoxicity study of blank liposomes and free PTX solvent on C6 cells ( $n = 3$ , mean  $\pm$  SD). Horizontal coordinate represents corresponding PTX concentrations of blank vehicles.

### 3.8. Cytotoxicity study in vitro

The cytotoxicity of different liposomes on C6 cells was evaluated using MTT assay. As shown in Fig. 9A, free PTX showed higher inhibition rate than PTX-PEG-lipo and PTX-RGD-lipo, because free drugs could be transported into the cells directly without a drug release process. Nevertheless, PTX-loaded R8-RGD-lipo and R8-lipo both exhibited stronger anti-proliferation effect than free PTX on C6 cells owing to their enhanced cellular uptake. The data showed that when the concentration of paclitaxel reached 5  $\mu\text{g/ml}$  or higher, the cell viabilities of PTX-R8-RGD-lipo and PTX-R8-lipo were too low to be measured accurately (lower than 5%) while nearly 20% of the cells in free PTX group still remained viable. Meanwhile, R8-RGD-lipo showed significant higher inhibition rate than R8-lipo under low PTX concentrations (lower than 1  $\mu\text{g/ml}$ ). Only 37.2% of the C6 cells stayed viable in the PTX-R8-RGD-lipo added group when the PTX concentration was as low as 0.1  $\mu\text{g/ml}$  while the cell viability rates of PTX-R8-lipo and free PTX were 47.5% and 46.6% respectively under the same PTX concentration, demonstrating that R8-RGD could notably enhance the cytotoxicity of drug loaded liposomes against C6 cells. On the other hand, the cytotoxicity of blank liposomes was also measured, and all these four kinds of blank liposomes exhibited no significant cytotoxicity (Fig. 9B) while free PTX solvent (ethanol-cremophor ELP 35 mixture,  $v/v = 1:1$ ) displayed an anti-proliferation effect as the concentration increased. Therefore our liposomal drug delivery systems were safe and nonvenomous to be further used *in vivo*.

### 3.9. Apoptosis study in vitro

Annexin V-FITC/PI apoptosis detection kit was used to study the cell apoptosis induced by PTX-loaded liposomes. Fig. 10B showed the percentage of apoptosis and necrotic cells treated with different PTX formulations. The percentage of apoptosis and necrotic cells was  $18.85 \pm 0.49\%$  for free PTX,  $13.70 \pm 0.71\%$  for PTX-PEG-lipo,  $38.30 \pm 3.11\%$  for PTX-R8-RGD-lipo,  $20.5 \pm 0.57\%$

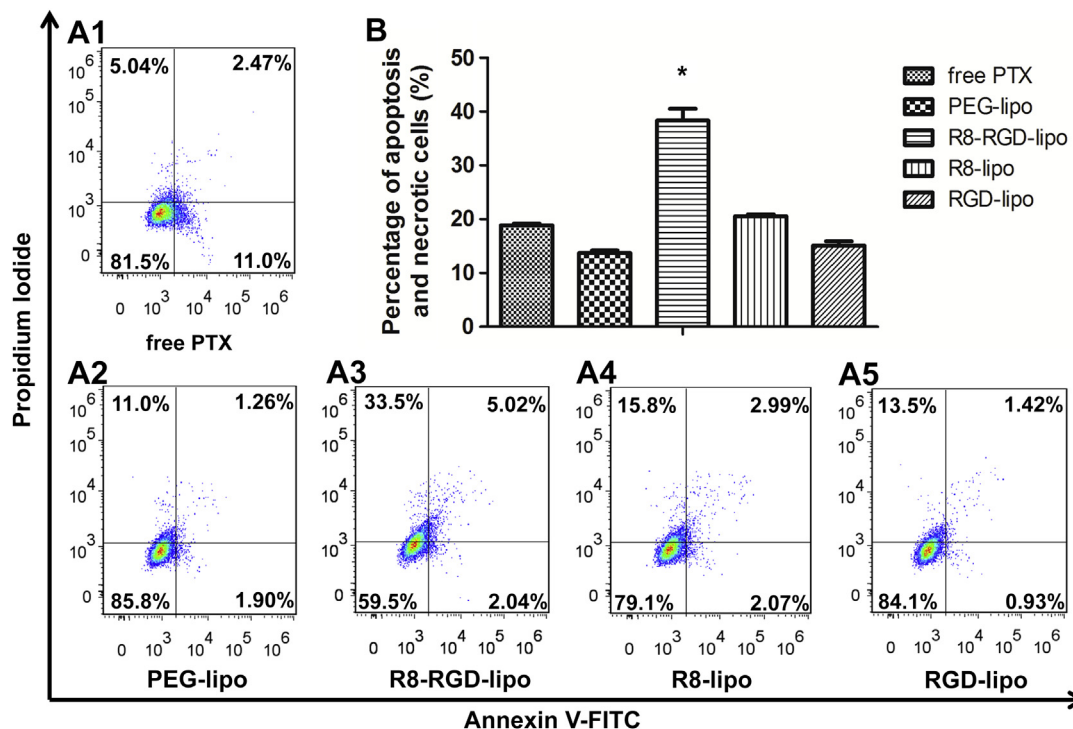


**Fig. 10.** The apoptosis study of C6 cells after incubation with free PTX (A1), PTX-PEG-lipo (A2), PTX-R8-RGD-lipo (A3); PTX-R8-lipo (A4) and PTX-RGD-lipo (A5). (B) The percentage of apoptosis and necrotic cells after free PTX and PTX-loaded liposomes treatment ( $n = 3$ , mean  $\pm$  SD), \*represents  $p < 0.05$  versus other groups.

for R8-lipo and  $15.05 \pm 71.20\%$  for RGD-lipo, respectively. R8-RGD modified PTX loaded liposomes induced significant stronger cell apoptosis effect. The cytotoxicity and apoptosis study of PTX formations confirmed that R8-RGD could remarkably improve the cellular internalization of drug delivery systems, release more therapeutic agents into the cytoplasm and achieve stronger inhibition effect *in vitro*.

### 3.10. *In vivo* imaging and glioma distribution

C6 glioma bearing bab/c mice were used to estimate the glioma targeting efficiency of different liposomes. Fig. 11A showed the *in vivo* images of intracranial C6 glioma bearing mice at different time points after systemic administration of DiR-loaded liposomes. The mice were sacrificed at pre-determined time points, then the brains, hearts, livers, spleens, lungs and kidneys were harvested and pictured. *Ex vivo* images of the brains were exhibited in Fig. 11B and other organs were shown in Supplementary Information Fig. S3. It was perspicuously observed that the fluorescence signal of R8-RGD-lipo in the brain was stronger than other groups from 1 h to 24 h after systemic administration (Fig. 11A), displaying the strongest BBB transporting capability of R8-RGD. Blood-brain barrier is known to be negative charged, thus R8-lipo also exhibited a strong BBB penetrating ability as the positive charge of poly-arginine could induce an adsorptive-mediated transcytosis [10,40,55]. However, at 1 h and 4 h after injection, strong fluorescence signal of R8-lipo was also found distributing in the liver and finally no obvious signal was observed all over the mice body in the R8-lipo group 24 h after systemic administration. This was due to the fact that positively charged R8 peptide could be easily bound to proteins in the circulatory system, recognized by the reticuloendothelial system and finally eliminated quickly [56]. *Ex vivo* images of harvested organs also

confirmed that more R8-lipo were delivered to the liver compared to other groups (See Supplementary Information Fig. S3). However, when R8 was conjugated to a cyclic RGD peptide to form a tandem peptide, the liver distribution of liposomes decreased a lot. Moreover, as shown in the *ex vivo* images of the glioma bearing brains (Fig. 11B), R8-RGD-lipo and R8-lipo both reached the maximum distribution in the brains 8 h after injection, but R8-RGD-lipo could selectively accumulate in the glioma foci instead of distributing uniformly in the whole brain. This property would efficiently reduce unwanted side effects to normal brain tissues. Besides, strong fluorescence signal of R8-RGD-lipo in the glioma foci could maintain till 24 h after injection while the signal of R8-lipo decreased a lot.

CPP have been widely investigated as drug delivery vectors or ligands for nearly 20 years. An important hurdle of CPP-mediated drug delivery systems is the general lack of cell or tissue specificity while been used *in vivo* [57–59]. Thus the therapeutic efficacy will decrease while the cytotoxicity against normal tissues becomes a potential threat due to the uncontrollable distribution during the treatment of CPP-modified cargos [57]. To overcome this impediment, researches established a dual-ligand system which had a specific ligand and a CPP decorated on a single drug carrier and had already proved their synergetic targeting effect to tumor [28]. A transferrin/poly-arginine dual targeting liposomal system had also been used for gene delivery into the brain [55]. However, these systems need to conjugate two kinds of ligands to one single nanoparticle, which pulls in more factors that may influence the drug delivery system during the preparation of nanoparticles. Thus, it is more potential to simplify the modifications of nanoparticles while the targeting ability is maintained. In this part, by investigating the glioma targeting effect of the tandem peptide R8-RGD using *in vivo* images, we proved that the synergetic targeting effect still existed while R8 and RGD were conjugated to form a single ligand.

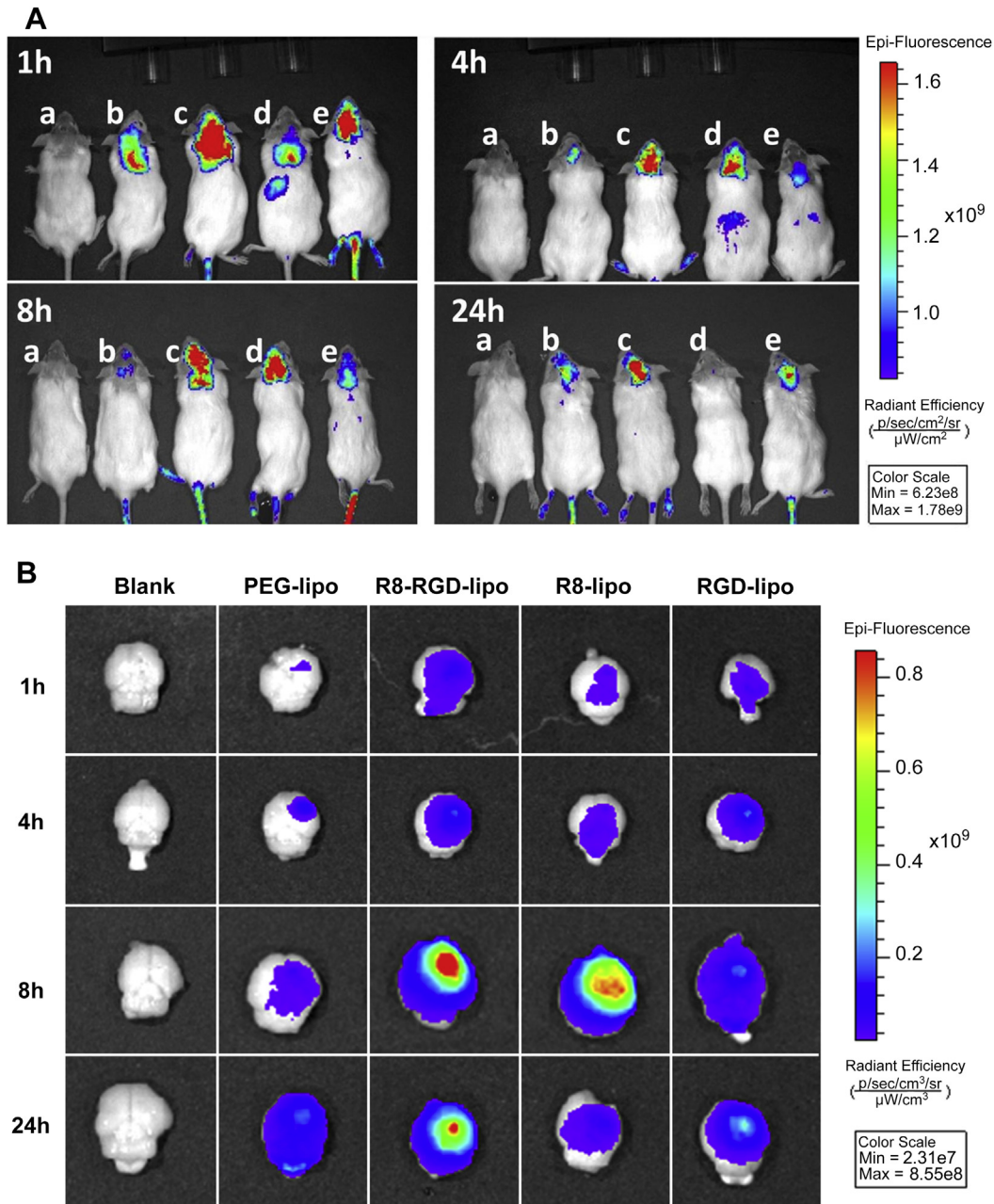


**Fig. 11.** (A) *In vivo* images of intracranial C6 glioma bearing mice at different time points after systemic administration of DiI-loaded liposomes (a = blank, b = PEG-lipo, c = R8-RGD-lipo, d = R8-lipo, e = RGD-lipo). (B) *Ex vivo* images of the brains.

*In vivo* glioma targeting and permeating capability of liposomes were studied here by confocal microscopy analysis. As shown in Fig. 12, 8 h after the injection of DiI-loaded liposomes, PEG-lipo and RGD-lipo could hardly be observed in the glioma tissue. Only a slight accumulation of R8-lipo was detected while an obvious strong fluorescence signal colocalized with the tumor cells was observed in the section of R8-RGD-lipo group. R8-RGD could enrich liposomes at the glioma foci and achieve wide distribution in the glioma tissue. These *in vivo* imaging and glioma distribution results further proved that R8-RGD possessed a high BBB transporting ability, a selective glioma targeting ability and a tumor penetrating ability not only *in vitro* but also *in vivo*, and this multifunctional property could exhibit superiority in the anti-tumor therapy.

### 3.11. Anti-glioma efficacy

The anti-glioma effects of different PTX formulations were evaluated on intracranial C6 glioma bearing mice. The enhanced glioma accumulation and penetration induced by R8-RGD led to a prolonged survival time. As shown in Fig. 13, PTX-R8-RGD-lipo group achieved an improved anti-glioma effect by prolonging the medium survival time to 48 days (Table 2), significantly longer than the other groups treated with saline (26 days), free PTX (32 days), PTX-PEG-lipo (39 days), PTX-R8-lipo (36 days) and PTX-RGD-lipo (38 days). Thus the multifunctional peptide R8-RGD modified drug loaded liposome was proved to be a potential drug delivery system for glioma treatment.

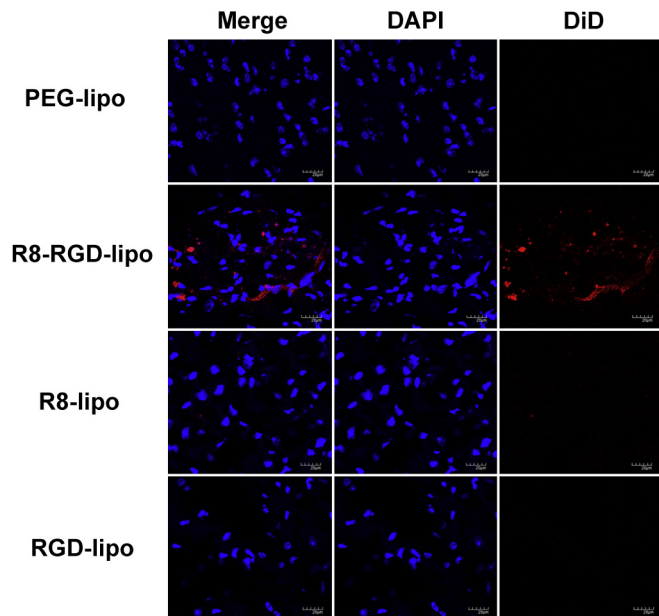


**Fig. 12.** CLSM images of glioma sections from C6 bearing Balb/c mice 8 h after systemic administration of DiD-loaded liposomes (red). Nuclei were stained with DAPI (blue). (For interpretation of the references to color in this figure legend, the reader is referred to the web version of this article.)

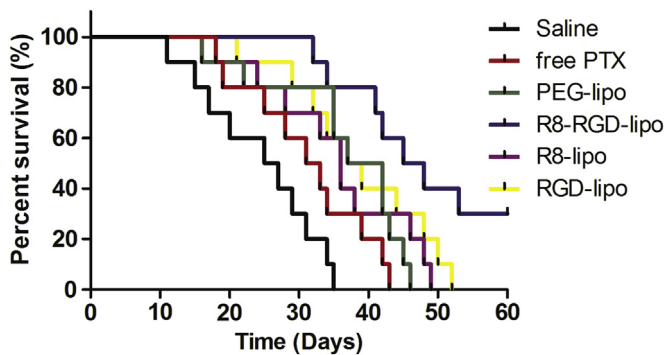


**Fig. 13.** Kaplan–Meier survival curve of intracranial C6 glioma bearing mice treated with different PTX formulations ( $n = 10$ ).

**Table 2**

The median survival time of the glioma bearing mice treated with different PTX formulations (<sup>a</sup> $p < 0.05$  versus saline, <sup>b</sup> $p < 0.05$  versus free PTX, <sup>c</sup> $p < 0.05$  versus PEG-lipo, <sup>d</sup> $p < 0.05$  versus R8-lipo, <sup>e</sup> $p < 0.05$  versus RGD-lipo).

Group	Median (day)	Standard error	95% confidence interval	Significant	Increased survival time
Saline	26	5.5	14.1–35.8	—	—
Free PTX	32	3.9	23.2–38.7	a	23%
PEG-lipo	39	3.6	29.7–44.2	a	50%
R8-RGD-lipo	48	4.7	35.7–54.3	a,b,c,d,e	85%
R8-lipo	36	2.3	31.4–40.5	a	38%
RGD-lipo	38	3.9	29.2–44.7	a,b	46%

#### 4. Conclusion

We here successfully developed a tandem peptide R8-RGD modified liposomal drug delivery system for anti-glioma therapy. R8-RGD, as a multifunctional ligand, displayed high BBB

transporting, selectively glioma targeting and tumor penetrating capabilities. Based on all the studies in this report, we claimed the multifunctional tandem peptide R8-RGD as an effective ligand for BBB and glioma targeting, and R8-RGD modified liposomes as a potential anti-tumor drug delivery system.

#### Acknowledgments

The work was funded by the National Natural Science Foundation of China (81373337) and the National Basic Research Program of China (973 Program, 2013CB932504).

#### Appendix A. Supplementary data

Supplementary data related to this article can be found at <http://dx.doi.org/10.1016/j.biomaterials.2014.02.031>.

#### References

- [1] Deeken JF, Loscher W. The blood–brain barrier and cancer: transporters, treatment, and Trojan horses. *Clin Cancer Res* 2007;13:1663–74.
- [2] Serwer LP, James CD. Challenges in drug delivery to tumors of the central nervous system: an overview of pharmacological and surgical considerations. *Adv Drug Deliv Rev* 2012;64:590–7.
- [3] Gao H, Jiang X. Progress on the diagnosis and evaluation of brain tumors. *Cancer Imaging* 2013;13(4):466–81.
- [4] Gao H, Pang Z, Jiang X. Targeted delivery of nano-therapeutics for major disorders of the central nervous system. *Pharm Res* 2013;30(10):2485–98.
- [5] Groothuis DR. The blood–brain and blood–tumor barriers: a review of strategies for increasing drug delivery. *Neuro-Oncology* 2000;2(1):45–59.
- [6] Zhan C, Wei X, Qian J, Feng L, Zhu J, Lu W. Co-delivery of TRAIL gene enhances the anti-glioblastoma effect of paclitaxel *in vitro* and *in vivo*. *J Control Release* 2012;160(3):630–6.
- [7] Sarin H, Kanevsky AS, Wu H, Sousa AA, Wilson CM, Aronova MA, et al. Physiologic upper limit of pore size in the blood–tumor barrier of malignant solid tumors. *J Transl Med* 2009;7(51):1–13.
- [8] Lamfers ML, Idema S, Bosscher L, Heukelom S, Moeniralm S, van der Meulen-Muileman IH, et al. Differential effects of combined Ad5-Δ24RGD and radiation therapy in *in vitro* versus *in vivo* models of malignant glioma. *Clin Cancer Res* 2007;13:7451–8.
- [9] Jiang X, Xin H, Gu J, Xu X, Xia W, Chen S, et al. Solid tumor penetration by integrin-mediated pegylated poly(trimethylene carbonate) nanoparticles loaded with paclitaxel. *Biomaterials* 2013;34:1739–46.
- [10] Chen Y, Liu L. Modern methods for delivery of drugs across the blood–brain barrier. *Adv Drug Deliv Rev* 2012;64:640–65.
- [11] Gao H, Yang Z, Cao S, Xiong Y, Zhang S, Pang Z, et al. Tumor cells and neovasculature dual targeting delivery for glioblastoma treatment. *Biomaterials* 2014;35(7):2374–82.
- [12] Lu W, Xiong C, Zhang R, Shi L, Huang M, Zhang G, et al. Receptor-mediated transcytosis: a mechanism for active extravascular transport of nanoparticles in solid tumors. *J Control Release* 2012;161:959–66.
- [13] Veiseh O, Sun C, Fang C, Bhattarai N, Gunn J, Kievit F, et al. Specific targeting of brain tumors with an optical/magnetic resonance imaging nanoprobe across the blood–brain barrier. *Cancer Res* 2009;69(15):6200–7.
- [14] Chen H, Tang L, Qin Y, Yin Y, Tang J, Tang W, et al. Lactoferrin-modified procatenionic liposomes as a novel drug carrier for brain delivery. *Eur J Pharm Sci* 2010;40:94–102.
- [15] Gao H, Yang Z, Zhang S, Cao S, Pang Z, Yang X, et al. Glioma-homing peptide with a cell-penetrating effect for targeting delivery with enhanced glioma localization, penetration and suppression of glioma growth. *J Control Release* 2013;172(3):921–8.
- [16] Gao H, Qian J, Cao S, Yang Z, Pang Z, Pan S, et al. Precise glioma targeting of and penetration by aptamer and peptide dual-functioned nanoparticles. *Biomaterials* 2012;33(20):5115–23.
- [17] Beduneau A, Saulnier P, Benoit JP. Active targeting of brain tumors using nanocarriers. *Biomaterials* 2007;28:4947–67.
- [18] Gao H, Pan S, Yang Z, Cao S, Chen C, Jiang X, et al. A cascade targeting strategy for brain neuroglial cells employing nanoparticles modified with angiopep-2 peptide and EGFP-EGF1 protein. *Biomaterials* 2011;32(33):8669–75.
- [19] Milletti F. Cell-penetrating peptides: classes, origin, and current landscape. *Drug Discov Today* 2012;17(15–16):850–60.
- [20] Mae M, Langel U. Cell-penetrating peptides as vectors for peptide, protein and oligonucleotide delivery. *Curr Opin Pharmacol* 2006;6:509–14.
- [21] Qin Y, Chen H, Yuan W, Kuai R, Zhang Q, Xie F, et al. Liposome formulated with TAT-modified cholesterol for enhancing the brain delivery. *Int J Pharm* 2011;419:85–95.
- [22] Qin Y, Chen H, Zhang Q, Wang X, Yuan W, Kuai R, et al. Liposome formulated with TAT-modified cholesterol for improving brain delivery and therapeutic efficacy on brain glioma in animals. *Int J Pharm* 2011;420:304–12.

- [23] Ren Y, Hauert S, Lo JH, Bhatia SN. Identification and characterization of receptor-specific peptides for siRNA delivery. *ACS Nano* 2012;6(10):8620–31.
- [24] Laakkonen P, Porkka K, Hoffman JA, Ruoslahti E. A tumor-homing peptide with a targeting specificity related to lymphatic vessels. *Nat Med* 2002;8(7):751–5.
- [25] Fang B, Jiang L, Zhang M, Ren FZ. A novel cell-penetrating peptide TAT-A1 delivers siRNA into tumor cells selectively. *Biochimie* 2013;95(2):251–7.
- [26] Chen JX, Wang HY, Li C, Han K, Zhang XZ, Zhuo RX. Construction of surfactant-like tetra-tail amphiphilic peptide with RGD ligand for encapsulation of porphyrin for photodynamic therapy. *Biomaterials* 2011;32:1678–84.
- [27] Barczyk M, Carracedo S, Gullberg D. Integrins. *Cell Tissue Res* 2010;339:269–80.
- [28] Kibria G, Hatakeyama H, Ohga N, Hida K, Harashima H. Dual-ligand modification of PEGylated liposomes shows better cell selectivity and efficient gene delivery. *J Control Release* 2011;153:141–8.
- [29] Magnon C, Galaup A, Mullan B, Rouffiac V, Bidart JM, Griscell F, et al. Canstatin acts on endothelial and tumor cells via mitochondrial damage initiated through interaction with  $\alpha_v\beta_3$  and  $\alpha_v\beta_5$  integrins. *Cancer Res* 2005;65(10):4353–61.
- [30] Chen X, Park R, Shahinian AH, Tohme M, Khankaldyyan V, Bozorgzadeh MH, et al.  $^{18}\text{F}$ -labeled RGD peptide: initial evaluation for imaging brain tumor angiogenesis. *Nucl Med Biol* 2004;31:179–89.
- [31] Gao H, Xiong Y, Zhang S, Yang Z, Cao S, Jiang X. RGD and interleukin-13 peptide functionalized nanoparticles for enhanced glioblastoma cells and neovasculature dual targeting delivery and elevated tumor penetration. *Mol Pharm*; 2014. <http://dx.doi.org/10.1021/mp400751g>.
- [32] Yan H, Wang L, Wang J, Weng X, Lei H, Wang X, et al. Two-order targeted brain tumor imaging by using an optical/paramagnetic nanoprobe across the blood brain barrier. *ACS Nano* 2012;6(1):410–20.
- [33] Cheng Y, Morshed RA, Auffinger B, Tobias AL, Lesniak MS. Multifunctional nanoparticles for brain tumor imaging and therapy. *Adv Drug Deliv Rev*. <http://dx.doi.org/10.1016/j.addr.2013.09.006>; 2013.
- [34] Seftor RE, Seftor EA, Stetler-Stevenson WG, Hendrix MJ. The 72kDa type IV collagenase is modulated via differential expression of  $\alpha_v\beta_3$  and  $\alpha_5\beta_1$  integrins during human melanoma cell invasion. *Cancer Res* 1993;53:3411–5.
- [35] Ballestrem C, Hinz B, Imhof BA, Wehrle-Haller B. Marching at the front and dragging behind: differential  $\alpha_v\beta_3$  integrin turnover regulates focal adhesion behavior. *J Cell Biol* 2001;155:1319–32.
- [36] Dearing JL, Barnes JW, Panigrahy D, Zimmerman RE, Fahey F, Treves ST, et al. Specific uptake of  $^{99\text{m}}\text{Tc}$ -NC100692, an  $\alpha_v\beta_3$ -targeted imaging probe, in subcutaneous and orthotopic tumors. *Nucl Med Biol* 2013;40:788–94.
- [37] Brown RC, Morris AP, O'Neil RG. Tight junction protein expression and barrier properties of immortalized mouse brain microvessel endothelial cells. *Brain Res* 2007;1130:17–30.
- [38] Simon MJ, Kang WH, Gao S, Banta S, Morrison 3rd B. Increased delivery of TAT across an endothelial monolayer following ischemic injury. *Neurosci Lett* 2010;486:1–4.
- [39] Svensen N, Walton JG, Bradley M. Peptides for cell-selective drug delivery. *Trends Pharmacol Sci* 2012;33(4):186–92.
- [40] Yin Y, Wu X, Yang Z, Zhao J, Wang X, Zhang Q, et al. The potential efficacy of R8-modified paclitaxel-loaded liposomes on pulmonary arterial hypertension. *Pharm Res* 2013;30:2050–62.
- [41] Kawaguchi Y, Tanaka G, Nakase I, Imanishi M, Chiba J, Hatanaka Y, et al. Identification of cellular proteins interacting with octaarginine (R8) cell-penetrating peptide by photo-crosslinking. *Bioorg Med Chem Lett* 2013;23:3738–40.
- [42] Biswas S, Deshpande PP, Perche F, Dodwadkar NS, Sane SD, Torchilin VP. Octa-arginine-modified pegylated liposomal doxorubicin: an effective treatment strategy for non-small cell lung cancer. *Cancer Lett* 2013;335:191–200.
- [43] Gong C, Li X, Xu L, Zhang YH. Target delivery of a gene into the brain using the RVG29-oligoarginine peptide. *Biomaterials* 2012;33:3456–63.
- [44] Gao H, Yang Z, Zhang S, Cao S, Shen S, Pang Z, et al. Ligand modified nanoparticles increases cell uptake, alters endocytosis and elevates glioma distribution and internalization. *Sci Rep* 2013;3:2534.
- [45] Gao H, Yang Z, Zhang S, Pang Z, Jiang X. Internalization and subcellular fate of aptamer and peptide dual-functioned nanoparticles. *J Drug Target*; 2014. <http://dx.doi.org/10.3109/1061186X.2014.886038>.
- [46] Nichols B. Caveosomes and endocytosis of lipid rafts. *J Cell Sci* 2003;116(23):4707–14.
- [47] Du W, Fan Y, Zheng N, He B, Yuan L, Zhang H, et al. Transferrin receptor specific nanocarriers conjugated with functional 7peptide for oral drug delivery. *Biomaterials* 2013;34:794–806.
- [48] Diaz R, Mayorga L, Stahl P. *In vitro* fusion of endosomes following receptor-mediated endocytosis. *J Biol Chem* 1988;263(13):6093–100.
- [49] Wender PA, Gallihier WC, Goun EA, Jones LR, Pillow TH. The design of guanidinium-rich transporters and their internalization mechanisms. *Adv Drug Deliv Rev* 2008;60:452–72.
- [50] Futaki S, Suzuki T, Ohashi W, Yagami T, Tanaka S, Ueda K, et al. Arginine-rich peptides: an abundant source of membrane-permeable peptides having potential as carriers for intracellular protein delivery. *J Biol Chem* 2001;276(8):5836–40.
- [51] Cairns R, Papandreou I, Denko N. Overcoming physiologic barriers to cancer treatment by molecularly targeting the tumor microenvironment. *Mol Cancer Res* 2006;4(2):61–70.
- [52] Jain RK. Delivery of molecular and cellular medicine to solid tumors. *Adv Drug Deliv Rev* 2012;64:353–65.
- [53] Gao H, Qian J, Yang Z, Pang Z, Xi Z, Cao S, et al. Whole-cell SELEX aptamer-functionalised poly(ethyleneglycol)-poly( $\epsilon$ -caprolactone) nanoparticles for enhanced targeted glioblastoma therapy. *Biomaterials* 2012;33(26):6264–72.
- [54] Gao H, Yang Z, Zhang S, Pang Z, Liu Q, Jiang X. Study and evaluation of mechanisms of dual targeting drug delivery system with tumor microenvironment assays compared with normal assays. *Acta Biomater* 2014;10(2):858–67.
- [55] Sharma G, Modgil A, Layek B, Arora K, Sun C, Law B, et al. Cell penetrating peptide tethered bi-ligand liposomes for delivery to brain *in vivo*: bio-distribution and transfection. *J Control Release* 2013;167:1–10.
- [56] Li SD, Huang L. Pharmacokinetics and biodistribution of nanoparticles. *Mol Pharm* 2008;5(4):496–504.
- [57] Huang Y, Jiang Y, Wang H, Wang J, Shin MC, Byun Y, et al. Curb challenges of the "Trojan Horse" approach: smart strategies in achieving effective yet safe cell-penetrating peptide-based drug delivery. *Adv Drug Deliv Rev* 2013;65:1299–315.
- [58] Lee SH, Castagner B, Leroux JC. Is there a future for cell-penetrating peptides in oligonucleotide delivery? *Eur J Pharm Biopharm* 2013;85:5–11.
- [59] Bechara C, Sagan S. Cell-penetrating peptides: 20 years later, what do we stand? *FEBS Lett* 2013;587:1693–702.